A study of the wear performance of duplex treated commercial low-alloy steel against alumina and WC balls

Nasser Eddine Beliardouh [a,*], Corinne Nouveau [b], Michael J. Walock [c], Philippe Jacquet [b]

[a] Laboratoire Ingénierie des Surfaces (LIS), Université Badji Mokhtar, BP 12, Annaba 23000, Algeria
[b] Arts et Métiers ParisTech, Laboratoire Bourguignon des Matériaux et Procédés (LaBoMaP), Rue Porte de Paris, 71250 Cluny, France
[c] University of Alabama at Birmingham (UAB), Department of Physics, CH 310, 1720 2nd Ave S, Birmingham, AL 35294-1170, USA

ARTICLE INFO

Article history:
Received 21 June 2014
Accepted in revised form 19 October 2014
Available online 23 October 2014

Keywords:
Duplex treatment
Sputtering
Cr–(WC–Co) coating
Wear
Tribology

ABSTRACT

The objective of this work is to study the improvement of the tribological properties of low alloy steel using a duplex treatment of low pressure carburizing and the deposition of a Cr–(WC–Co) coating by dual RF magnetron sputtering. The treatments result in a 500 μm thick carburized layer and a sputtered coating thickness of ~2 μm. Tribological tests were made with a ball-on-disk tribometer under dry conditions with low load and low speed. The worn surfaces of the disk, the wear counterpart, and resulting debris were analyzed by X-ray diffraction, optical microscopy, optical profilometry, and a scanning electron microscope equipped with an energy-dispersive X-ray spectrometer. The wear performance of the samples was evaluated in terms of wear rates and friction coefficients during the sliding processes against two different counterparts. Experimental results have shown that sliding wear, of the investigated duplex treated low alloy steels, is strongly dependent on the counterface materials. Under testing conditions, the overall wear performance of a Cr–WC coating (Cr/W ratio of 1.12:1) deposited onto the surface of a carburized low alloy steel (0.61 wt.% C; HV = 654 ± 5) can be recommended as the best. The duplex-treated samples suffered severe, concentrated wear when against alumina. This wear is characterized by a combination of delamination, mild abrasion and oxidative wear. However, the wear mechanism seems to be oxidative and adhesive when against WC balls.

1. Introduction

As a result of the increased demand for the protection of tools, machine parts, and other devices through surface modification, a wide range of hard coatings and their deposition technology are available. Choosing the proper substrate, coating material and deposition/surface treatment method can dramatically improve the service life of a mechanical component/system, but performance is never the only consideration. Economic and ecological considerations must also be taken into account. For example, changing the substrate material from expensive alloyed steel to cheaper low-alloyed steel can have significant improvements in material availability and reduced production costs [1].

Yet, the mechanical and tribological properties of hard coatings may be reduced when applied to low-alloy steels. Therefore, interfacial engineering is necessary to enhance the tribo-mechanical properties of the coating/substrate system. Duplex treatments have been applied to improve adhesion between different steel substrates and various hard coatings, and to enhance the tribological performance [2]. Duplex treatments can be classified as modern technological processes, respecting the environment while ensuring the required properties. Duplex treatments of steel surfaces consist of a thermo-chemical treatment (such as nitriding or carburizing), followed by a coating deposition. The coatings are produced by various techniques, such as chemical vapor deposition (CVD), physical vapor deposition (PVD), plasma assisted CVD (PACVD) or plasma assisted PVD (PAPVD) [3,4]. Other duplex processes, such as using thermo-reactive diffusion techniques, chromizing, and nitriding, have also been studied in the literature [5–7]. All of these technological processes can be applied to carbides, nitrides, oxides and/or boride hard coatings on various steels and/or other substrates. In comparison to a single process, a duplex treatment can combine the strength and stiffness of the steel substrate with the tribological and/or electrochemical properties of the coating. Kessler et al. [8,9] present a series of combined processes, such as heat treatment + coating and coating + heat treatment, on different steel substrates. In these papers, they classify the different combinations of coatings/heat treatments and summarize the advantages/disadvantages of each combination.

Many chromium-based coatings have been studied during the last 20 years. For instance, ternary CrXN coatings (where X is a metal, such as Al, Mo, Ti, W…) can be obtained by reactive magnetron sputtering. They are a well-known group of hard and very stable nitride

* Corresponding author. Tel.: +213 0669731635.
E-mail addresses: beliardouh_23@yahoo.fr (N.E. Beliardouh), corinne.nouveau@ENSAM.EU (C. Nouveau), mwalock@uab.edu (M.J. Walock), philippe.jacquet@ecam.fr (P. Jacquet).

coatings. These coatings exhibit high micro-hardness, low thermal conductivity, good wear resistance, and excellent corrosion resistance [10,11]. Also, the friction and wear of single and multilayer films involving CrN against several materials, remain a subject of interest for several authors. It was established [12] that tribological behavior of CrN coating strongly depends on the microstructure and thickness in different tribo-pair systems. More recently, research conducted by [13] in the focus to predict the effect of high temperature on CrN coated tools wear performance, confirms the excellent thermal stability and wear resistance of CrN based coating.

Moreover, Cr-based coatings containing carbon are widely used as tribological coating materials in high-temperature applications [14–16]. According to Su et al. [17] and Jellad et al. [18], sputtered Cr–C films can be of practical interest in abrasive and dry-sliding wear protection applications; in particular, Cr_3C_2 presents excellent strength, hardness, and good corrosion-resistant properties [19–22].

The previous results on the properties of Cr-based PVD coatings and duplex treatments on steel tools were a good motivation to go further. While forming a good base of knowledge, these previous studies were mostly made for metal machining. Also, no duplex treatments, such as carburizing combined with Cr-based PVD coatings, were studied yet. Then it was obvious that the development of such work on the effect of carburizing and of carburizing + CrWC PVD coated steel, in the hopes of applying the obtained results for wood cutting tools, would be a significant research advance for the wood industry.

This paper will study the wear behavior of Cr–(WC–Co) films synthesized by dual RF magnetron sputtering on low-alloy steel. Results are presented as follows:

1) Optimization of the carburizing of the steel substrate and the necessary deposition conditions of Cr–(WC–Co) coatings for their application on wood machining tools.
2) Investigation of the wear resistance of the Cr–WC–Co coatings against different counterparts (Al_2O_3 and WC balls).

2. Materials and methods

2.1. Material

The substrate material considered in this study is a commercial low-alloy steel, DIN 18CrMo$_4$ (Mat. No. 1.7243). The chemical composition of the substrate is shown in Table 1. This steel has high mechanical strength, high fatigue resistance, and a low price. Indeed, with a carburizing cycle followed by quenching and annealing, this material presents a high superficial hardness with a good ductility at its core (bulk material). This material is commonly employed for machine devices working under surface wear and alternating shock conditions.

2.2. Low-pressure carburizing (LPC) treatments

The samples were cut cylindrical (Ø 20 × 5 mm height) with an aim for perfect parallelism on the surface. The resulting pieces were mechanically polished with P800 paper, ultrasonically cleaned with acetone, and finally introduced into a single-chamber industrial vacuum furnace "BMI" for carburizing. The chamber is pumped down to 10 Pa. This is followed by heating up to 900 °C (Fig. 1). The substrates were carburized with alternating boost/diffusion stages. The carburizing gas was ethylene (C_2H_4) under 1 kPa. The length of the "boost-diffusion" carburizing step for two different carburizing mixtures is optimally

Table 1
Chemical composition of 18CrMo$_4$ steel (wt.%)-balance is Fe.

C	Si	Mn	P	S	Cr	Mo
0.13 → 0.21	Max. 0.4	0.6 → 0.9	Max. 0.025	Max. 0.035	0.9 → 1.2	0.15 → 0.25

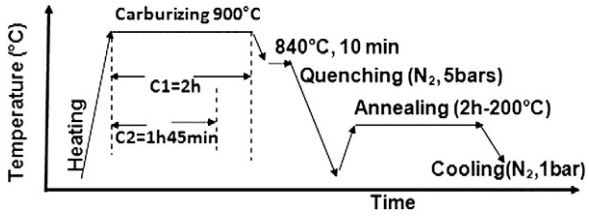

Fig. 1. Heat treatment diagram applied to carburize the 18CrMo$_4$ steel substrates.

selected on the basis of prior experimental data [23]. The total time intervals of the boost/diffusion stages were 120 min and 105 min for the first one (carburizing C1) and the second (carburizing C2), respectively.

After the carburizing process, samples are in-situ quenched in a high pressure N_2 environment (500 kPa), and subsequently annealed at 200 °C for 120 min. The samples were cooled down in a 100 kPa N_2 atmosphere. These carburized steels were characterized by scanning electron microscopy with energy-dispersive X-ray spectroscopy (SEM/EDS, JEOL JSM-5900LV), and optical microscopy (OM; Olympus VANOX-T). Vickers micro-hardness tests were performed to assess the role of the treatment on the modification of mechanical properties (LECO M-400-G micro hardness tester, 100 g applied load). The carbon content at the surface of samples was measured with the use of a LECO CS-200 Analyzer.

2.3. Deposition of coating

Cr–(WC–Co) coatings were prepared by reactive dual RF magnetron sputtering in a modified commercial system (Nordiko 3500, 13.56 MHz). Substrate to target distance was 80 mm and the residual pressure was 6×10^{-5} Pa. The 4-in targets were Cr (Neyco, purity of 99.95%) and WC–Co (Ampere, purity of 99.5%); the cemented WC target contained 6 wt.% Co. The substrates were chemically cleaned, followed by a 12 kV DC glow discharge pulsed plasma (25 ms on/50 ms off) for 5 min in an Argon atmosphere at 2 Pa. Substrates were heated to 300 °C to improve both adhesion and mechanical properties of the coatings. The Cr–(WC–Co) coatings were deposited at an argon working pressure of 1 Pa, the cemented-carbide target bias was −600 V, and the Cr target bias was −300 V for the F101 coating and −900 V for the F102 coating.

The coatings' structures were characterized by grazing incidence XRD (Philips X'pert with $\lambda_{Cu\text{-}K\alpha} = 0.15406$ nm), SEM observations and EDS microanalyses. The micro hardness of the layers was investigated by nanoindentation, with an indentation load ranging from 0 to 10 mN (MTS Nano-indenter XP, Berkovich indenter).

2.4. Wear tests

The wear resistance of the treatments has been studied with a pin-on-disk tribometer (CSM HT1000) and the Tribox 4.1.1 software under dry-sliding conditions at room temperature. The two standards for the pin-on-disk test are DIN 50324 and ASTM G 99–95a [24]. The counterparts were alumina (hardness H = 16.14 GPa; arithmetic average (R_a) and the root mean squared (RMS) surface roughness were 178 ± 0.03 (nm) and 256 ± 0.03 (nm), respectively) and WC–6% Co balls (H = 15 GPa; R_a = 125 (nm) and RMS = 173 ± 0.03 (nm)), supplied by CSM Instruments. These materials have a higher hardness than steel. Abrasion and shocks are expected during wood machining process thus they are quite suitable to test the wear resistance of coatings in this study. In addition, alumina is widely used as a counter-body because this system (alumina vs. hard coating based CrN) has already been proven to show higher wear resistance and significant differences in material behavior during sliding. This may be related to the high oxidation resistance and high surface chemical inertness of the Al_2O_3 ball [25].

Table 2
Wear test parameters and results of roughness measurements.

State of sample	Roughness (μm)		Static partner (Ø = 6 mm)	Parameters of test input
	Ra (±0.03)	RMS (±0.02)		
Carburizing(C1)	0.06	0.11	WC ball	Temperature 23–25 °C
Carburizing(C2)	0.05	0.07	Al_2O_3 ball	Humidity ~40%
C1 + coating F101	0.08	0.11		Speed sliding: 1 $cm \cdot s^{-1}$
C1 + coating F102	0.09	0.12		Load: 1 N
C2 + coating F101	0.10	0.13		Track radius: 4 mm
C2 + coating F102	0.09	0.11		Sliding distance: 200 m

WC–Co is used because it forms a 'quasi' self-mating tribo-couple with the Cr–(WC–Co) coatings. The literature about Cr(WC–Co)/(WC–Co) tribo system is very poor.

The selection of testing parameters, such as pin/disk materials, sliding distance, size of the ball, and applied load, has to be considered carefully because of their direct influence on the contact pressure at the ball/disk interface, especially during the run-in period [26].

The velocity and applied load have been chosen according to the limits of the tribometer and results from previous studies [27]. Specifically, the parameters were selected to limit the noise in the ball–disk assembly and the substantial adhesion of the material onto the disk/ball surface. A sliding distance of 200 m (time ~ 10^4 s) is sufficient to observe the wear of the entire coating (i.e. the complete removal of the coating from the substrate). The principal criterion for parameter selection was reproducibility of the results, and this combination of parameters guaranteed complete reproducibility of results. In this study, the measurements of the friction coefficient as a function of sliding distance are conducted at ambient laboratory conditions. Three wear tests were performed per sample. The wear test parameters and results of roughness measurements, are summarized in Table 2.

Prior to the wear tests, the samples and counterpart balls were ultrasonically cleaned in ethanol and dried with compressed air. The ball scars were observed by optical microscopy. The dimensions of the wear tracks (depth and width) were measured by 3D optical profilometry (Veeco, Wyko NT-1100). EDS microanalyses of the sample surface, the resultant wear tracks, and wear debris were collected during SEM examination of the surface morphology.

2.4.1. Wear rates

The wear rate is the rate of material removal or dimensional change (i.e. weight, volume, or thickness) during a given time or sliding distance [28,29]. To calculate the wear volume of the sample, additional measurements were performed. Wear volume loss of the sample was determined by measuring the cross-section area A of the wear track using optical profilometry. Thus, the wear volume loss V is obtained when the nominal circumference length of the track multiplies the cross-sectional area A. The specific wear rate of the disk (specimen) was estimated according to Eq. (1):

$$K = V/(L * N) \quad (1)$$

where V is the wear volume loss (mm^3), L is the sliding distance (m) and N is the normal load (N).

The quantification of the ball's wear volume is not easy; however, a semi-quantitative calculation was acceptable for comparison. The specific wear rate of the ball was estimated from the calculated volume loss at the spherical crown of the ball and Eq. (1). In addition to measurement of the balls' wear scars by optical microscopy, 3D analysis by optical profilometry was also used as suggested [30] and average values were calculated for the volume loss of the counterparts.

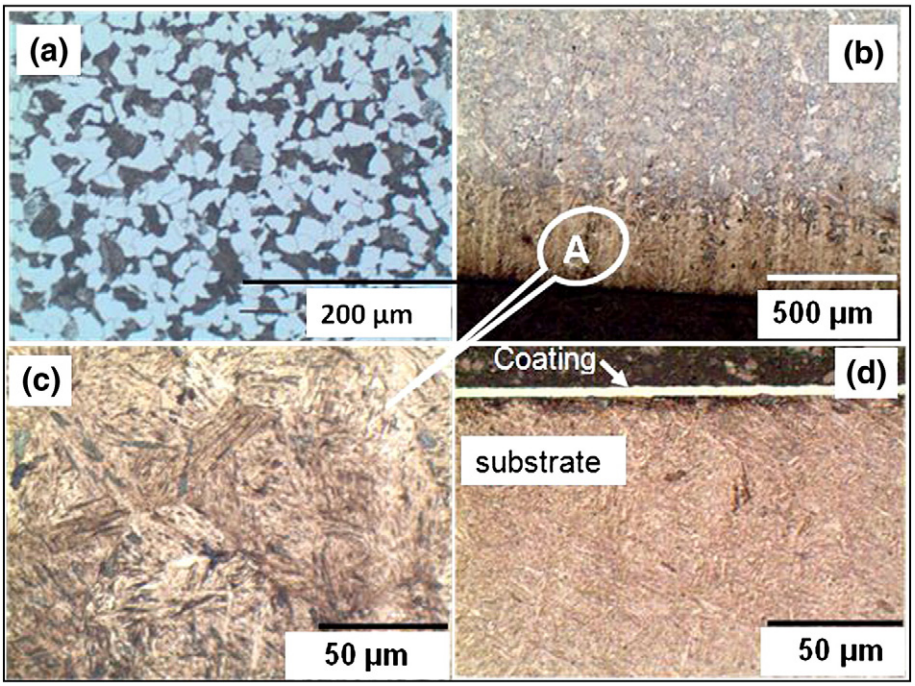

Fig. 2. Optical micrographs: (a) microstructure of the substrates before carburizing, (b) after carburizing, (c) region "A" and (d), cross section of a duplex treated steel.

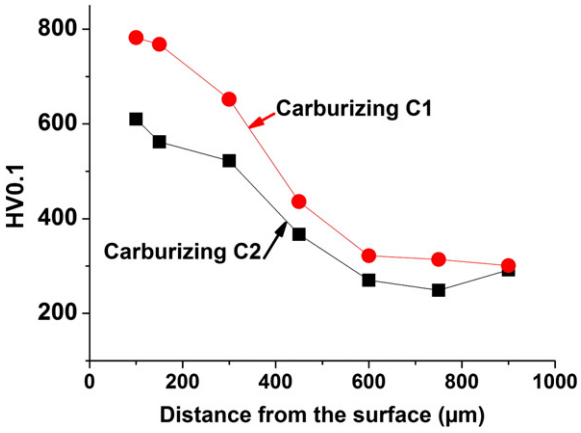

Fig. 3. Microhardness profiles of the C1 and C2 carburized substrates.

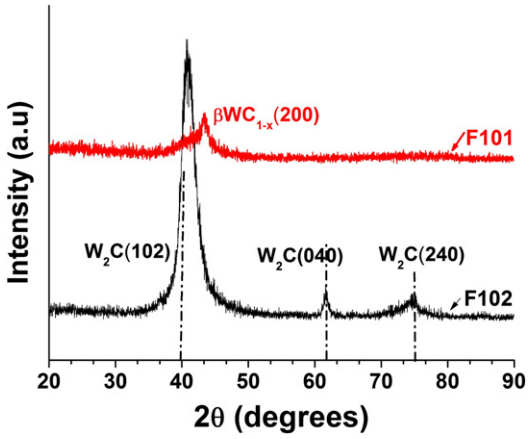

Fig. 4. X-ray diffraction patterns of Cr–(WC–Co) coatings; the substrate was Si(100) wafer.

3. Results and discussion

3.1. Carburizing

Surface micrographs before carburizing show a ferrite–pearlite structure (Fig. 2(a)). After carburizing, the treated samples exhibited the classical metallographic structure of carburized and heat treated steel [31]; the surface microstructure primarily consists of a dense layer of martensite and cementite (Fig. 2(b–c)). However, as a consequence of the fast phase transformation during cooling, some residual γ-austenite is still observed. Martensite and cementite (Fe_3C) phases are responsible for the surface hardness. The subsurface consists of an intermediate area composed of lamellar martensite, limited regions of proeutectoïd ferrite (white zones) and fine pearlite. The core of the steel is not affected by carbon diffusion; it contains proeutectoïd ferrite and low carbon martensite. OM and SEM estimate the depth of carburized layer which is about 500 μm, but it is difficult to distinguish the interface between the bulk steel and the intermediate layer. Therefore, the treated area presenting hardness greater than 550 HV is considered as the carburized layer.

Fig. 2(d) shows the cross-section of a duplex treated steel sample. The influence of the carburizing parameters on the superficial hardness of the steel has been studied by microhardness profiles (Fig. 3). The microhardness values decrease gradually from the surface of the sample to its core. The hardness of C1-treated sample (diffusion layer 200 μm thick and 0.67 wt.% of C) is HV = 768 ± 5 and the C2-treated sample (diffusion layer 350 μm thick and 0.61 wt.% of C) yields HV = 654 ± 5. The hardness of the core is around 300 HV for all samples.

3.2. Cr–(WC–Co) coatings

The chemical compositions (from EDS) and mechanical properties of the Cr–(WC–Co) coatings are presented in Table 3. As clearly seen, the mechanical properties of F101 ($H^3/E^2 = 0.175$) and F102 ($H^3/E^2 = 0.173$) are practically the same. The hardness and elastic modulus are determined by evaluating the respective nanoindentation curves at 5% of the total film thickness. This empirical rule of thumb yields results with minimal substrate effects. Besides, there is little difference between the chemical composition of F101 and F102; the Cr/W ratios are 1.53:1 and 1.12:1, respectively. This may explain the similarity in mechanical properties.

The diffraction patterns (Fig. 4) of the F101 coating shows only one broad diffraction peak, which may be the (200) peak of the cubic β-WC_{1-x} phase (JCPDS card number: 20-1316) at 43.65°. The diffraction patterns of the F102 coating showed a very intensive diffraction peak at 40.65° (102) and minor diffraction peaks at 61.61° (040) and 74.55° (240), which may come from the orthorhombic W_2C phase (JCPDS card number: 20-1315). Since the literature on this combination of materials is limited, it has been suggested in previous work [32] that the Cr–WC system consists of W–C and Cr–C phases. Thus, the breadth of the peaks may be the result of significant overlap between WC and Cr–C phases.

3.3. Tribology

The coefficient of friction is defined as the dimensionless ratio of the friction force between two bodies to the normal force pressing these bodies together. The static coefficient of friction is defined as the "friction coefficient corresponding to the maximum force that must be overcome to initiate macroscopic motion between two bodies" (ASTM G 40) [33].

Coatings used on tools employed in wood processing must meet very stringent property requirements, such as the appropriate microstructure and surface morphology, high hardness and Young's modulus, and good adhesion between coating/substrate. Another important trait is good tribological behavior, when in contact with the partner. These properties will have a direct impact on the tool wear.

The ball-on-disk sliding test is a simplified approach and widely used laboratory test that can be used to qualitatively assess tool wear. It has been employed by numerous authors to identify the friction coefficients in both metal and wood cutting processes [34–37]. Other industrial or semi-industrial (full scale) tests, such as turning tests [38,39] and cutting tests [37,40–42] are conducted as complementary and comparative tests to the pin/ball-on-disk (laboratory scale) tests. A good correlation between laboratory and industrial machining tests was reported [41,43]. However, tribological tests directly made on machine tools could be more interesting, but can also be very expensive [44].

Table 3
Chemical compositions and mechanical properties of CrWC–Co coatings.

Code	Chemical composition (wt.%); O_2 bal.				Thickness (μm)	Hardness (GPa)	Young's modulus (GPa)	H^3/E^2 ratio (GPa)	Critical load L_{c1}(N)
	C	Cr	Co	W					
F101	22.3	41.6	8.3	27.1	2.3	26.4	324.1	0.175	32.5
F102	23.3	35.4	8.8	31.8	2.2	26.7	331.3	0.173	32.5

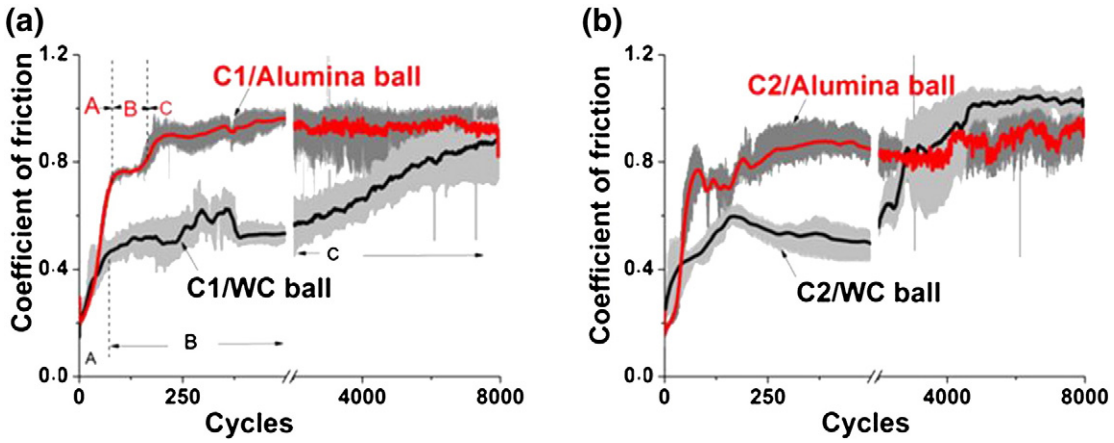

Fig. 5. Evolution of the coefficient of friction (COF) of carburized samples against alumina and WC counterparts.

3.3.1. Coefficients of friction (COFs)

3.3.1.1. Carburized samples. Fig. 5 shows the evolution of the coefficients of friction for the C1 and C2 samples, sliding against both alumina and WC balls. When sliding against alumina balls, three separate stages, indicated as zones A, B and C in Fig. 5(a), can be observed as a function of the number of cycles. The start of test corresponds to lower COF values due to the contaminated nature of the surface, i.e. 'surface pollution'. Immediately the COFs increase to higher values (0.7 and 0.8) for C1 and C2 respectively (Fig. 5(a–b)). Zone B (the transition stage) corresponds to an increase of the COF that is mostly due to an increase in the frictional force, as the counterpart deforms and fractures [45,46]. Once the asperities are smoothed out, zone C corresponds to the last ~2000 cycles. The values of the COF at the end of the tests are around 1.0 for both carburized samples.

When sliding against a cemented-WC ball, the COF of the carburized samples starts at 0.14 and 0.23 for C1 and C2, respectively. As with the last case, the same scheme appears, i.e. three separated zones: A, B and C. Zone A is followed by zone B (transitional zone) during the first 2000 cycles or so. Then, the COFs gradually increased and reach values up to ~0.8 for C1 and ~1.0 for C2 by the end of tests. This could be due to a change in the wear mechanism and may correspond to severe wear. In all cases, the friction against the cemented-WC counterpart seems to be less severe than against alumina counterpart. The COF values, in transitional zone, were around 0.5.

3.3.1.2. Duplex treated samples. The COF evolution of the duplex treated samples, which are in contact with alumina balls, is presented in Fig. 6. The evolution of the friction coefficients of the four tested samples is very similar: we observe a short first stage corresponding to the lowest COF values. This finishes after about a hundred cycles and may be considered as a running-in stage. After which, the COF gradually increases during the second stage, and then exhibits a relatively constant value. At the end of the tests, the COF values in all cases were approximately 0.8. And while tests with the alumina counterparts against carburized samples were relatively quiet, these tests of alumina counterparts

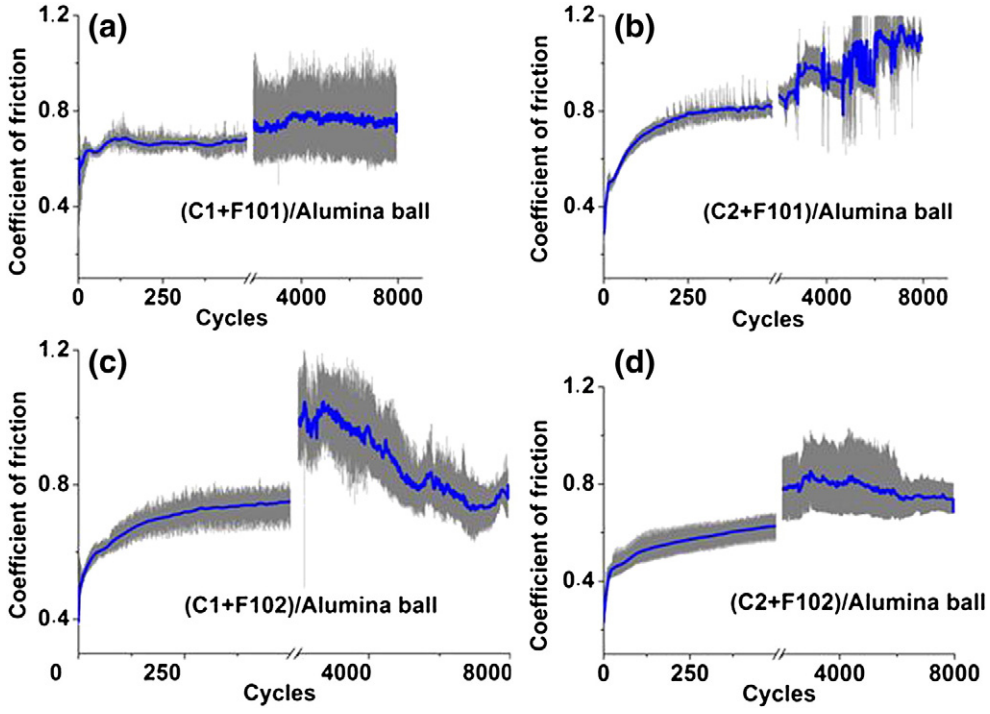

Fig. 6. Evolution of the coefficient of friction (COF) of duplex treated steel against an alumina counterpart.

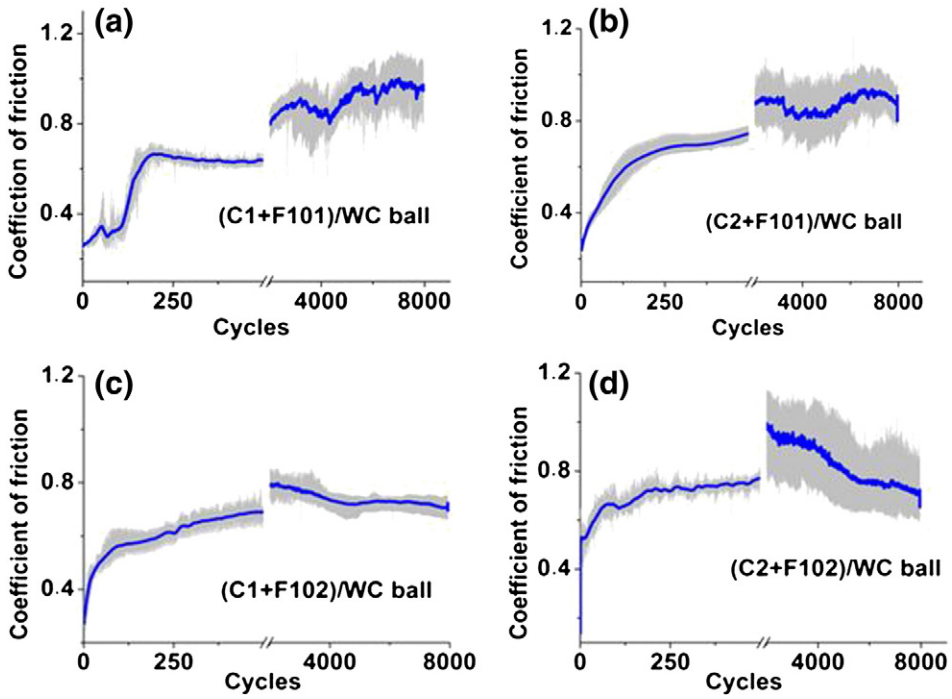

Fig. 7. Evolution of the coefficient of friction (COF) of duplex treated steel against a WC counterpart.

versus duplex treated samples produced an audible noise. The COF evolution of the coatings in contact with WC as counterpart is presented in Fig. 7. At the beginning of test, there is a short transitional stage of about 150 cycles. During this transitional stage, the COF increases slowly from 0.2 to 0.6, as shown in Fig. 7(a). Following this "run-in", the COF is constant and lower than those obtained against alumina balls. At the end of the third stage, all samples showed their highest COF; this may indicate that there are high adhesive forces in the contact zone. Similar to the test with the alumina counterpart, an audible noise was heard during the last cycles of the tests.

3.3.1.3. Comparing the friction behavior of the samples against different counterbodies. The averaged friction coefficients (Fig. 8) were obtained from statistics on the data collected during the stable period. These values were automatically calculated using the Tribox 4.1.1 software. The standard deviation σ ranged from 0.072 to 0.09 in steady-state region and the percentage error in the COF (for each tribo-pair) is about 3–4% after three tests. As can be seen in Fig. 8, the mean steady-state friction coefficient of the uncoated samples paired with the ceramic ball were the highest, while the uncoated/tungsten carbide tribo-pair exhibited the lowest values.

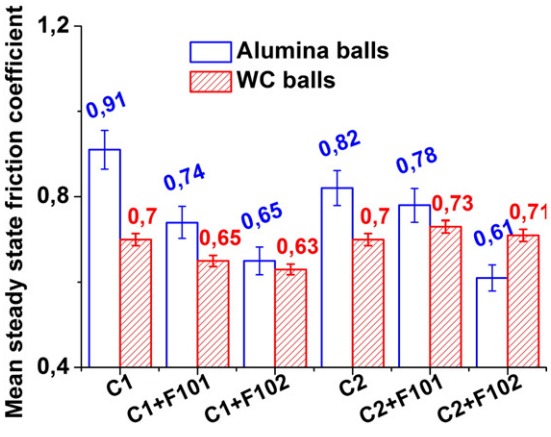

Fig. 8. Mean steady-state friction coefficients of duplex treated samples.

When against alumina balls, duplex treated samples (C2 + F102) show the lowest COF and (C2 + F101) the highest. When cemented-WC balls are the counter-bodies, the lowest values for the COFs were obtained in the case of (C1 + F102). $COF_{[C1\ +\ F102/(WC)]}$ is slightly lower than $COF_{[C1\ +\ F101/(WC]}$.

If only the friction behavior, under experimental conditions listed in Table 2, were considered, the carburized process C1 and coating F102 would be considered as the best combination for the (duplex treated samples)/(WC balls) tribo-pair. However, in the (duplex treated samples)/(Alumina balls) tribo-pair, F102 in combination with carburized process C2 is the best.

3.3.2. Wear analysis

3.3.2.1. Carburized samples. By analyzing the disk wear tracks and the counterpart wear scars, the general aspects of the wear mechanisms can be determined. Fig. 9(a–b) shows the wear tracks on carburized samples, obtained using alumina balls as the counterparts. The tribological tests have produced wear tracks via a "ploughing" of the sample surfaces. Within the wear tracks, EDS analysis indicates the presence of substrate elements (Fe, Cr) and oxygen. The wear debris is composed of the same chemical elements. Therefore, the wear mechanisms appear to be a combination of an oxidative and abrasive wear. Moreover, surface analyses of the balls (Fig. 9(c)) show a significant amount of adherent material containing O, Fe and Cr. From optical microscopy observations, some grooves are also detected on the surface of the alumina balls (Fig. 9(d)). These could be due to abrasive wear from the particles (three body wear) between the surfaces in contact.

As compared to the alumina counterparts, cemented carbide balls seem to produce less debris on the worn surfaces of the carburized samples, C1 and C2. SEM images (Fig. 10) show possible pores, agglomerated particles, debris, and some grooving of the surfaces in the wear track. EDS microanalysis indicates that the center of the track consists of metal oxides (Fe, Cr, W and O_2). Here, the only possible source for tungsten is the cemented carbide counterpart. So, the presence of tungsten in the disk wear track is indicative of adhesive wear. However,

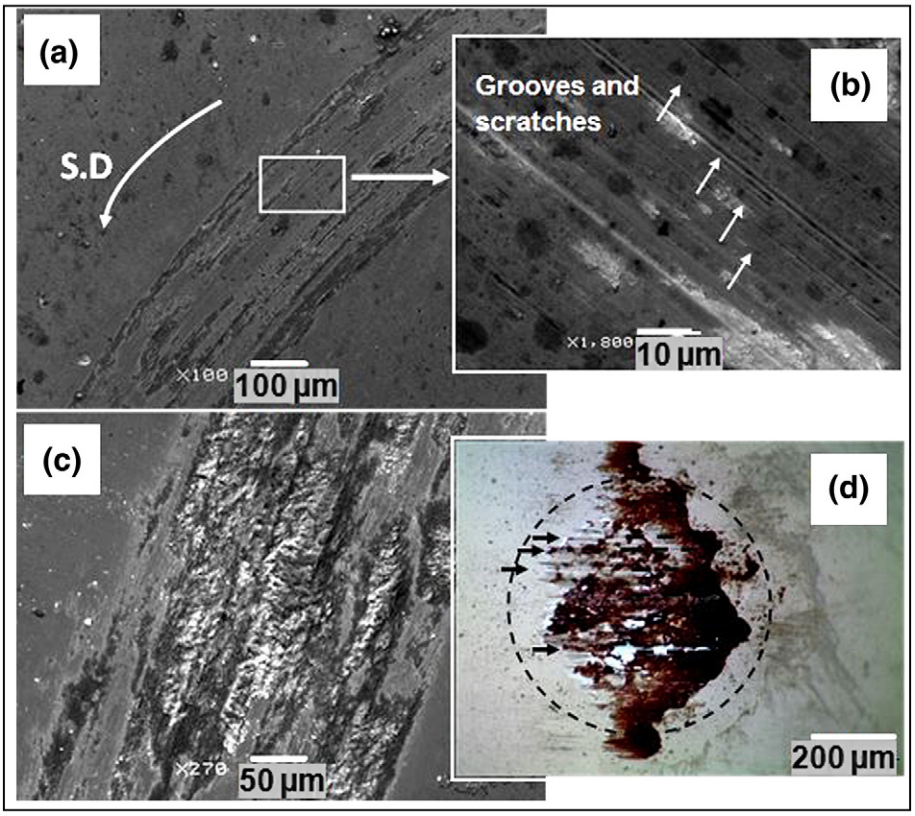

Fig. 9. (a–b) SEM image of the wear track of the carburized C1 sample after sliding against alumina ball (SD: sliding direction), (c) SEM image of the wear track of the carburized C2 sample against alumina ball, (d) optical image of the surface of the alumina ball; narrows point to grooves and furrows.

oxidative wear seems to be the main wear mechanism. This is supported by the presence of grooves and deep furrows on the WC counterparts (Fig. 10(d)). As the tests were performed, friction within the track would cause a local increase in temperature. This results in the formation of an oxide tribofilm. However, as the test continues and the number of sliding cycles increases, this oxide film becomes increasingly brittle. At some point during the tests, the film breaks up into wear debris (Fig. 10(c)). This wear debris leads to the severe abrasive wear observed on the cemented-WC counterparts.

In summary, alumina counterparts against carburized samples result in a combination of oxidative and abrasive wear mechanisms. Cemented carbide counterparts lead to oxidative and adhesive wear. While both counterparts experienced abrasive wear, the results are much more apparent on the surfaces of the WC balls.

3.3.2.2. Duplex treated samples vs. alumina ball. Fig. 11(a) shows an SEM image of the wear track on the C1 + F101 duplex treated sample. There appears to be debris on both sides of the track and within the track itself. It seems fairly well dispersed, and aligned with the sliding direction. The coating has been completely delaminated as shown by the EDS spectra (Fig. 11(b)). Indeed, there is a strong Fe peak within the spectrum. Some adhesive oxide layers may have formed during the test and the resulting debris has been pushed to the outward edges of the wear track.

The C1 + F102 duplex treated sample surface (Fig. 11(c)) shows a very different wear track than the previous sample. The track is clean and smooth, with only a small amount of debris in the track. Nevertheless, iron is still detected by EDS within the wear track of this sample, but its intensity is lower than in the previous duplex treated sample. It appears that the coating has not been completely destroyed, but it has undergone significant thinning. The analysis also shows the presence of oxides within the wear track, indicated by the dark regions in Fig. 11(d) (circled). Moreover, there are several cracks that have started to develop in the center of the wear track.

Finally, these two duplex treated samples show different states of wear after a sliding distance of 200 m. The C1 + F101 duplex treated sample shows severe wear as characterized by the dark and rougher wear track surface. And, an oxidative wear occurred for the C1 + F102 duplex treated sample as characterized by the smooth and clean wear track. SEM images of the wear tracks for the C2 + F101 and the C2 + F102 duplex treated samples are shown in Fig. 12. Cracking and delamination for both coated samples are observed. However, there is less wear debris along the wear track on the C2 + F102 duplex treated sample (Fig. 12(c–d)). EDS microanalysis revealed that the wear particles contain transition metals (such as Fe, Cr and/or W) and oxygen. Oxidative wear appears to be the main wear process.

Indeed, strain hardening from the tribological tests appears to have transformed the initial microstructure of the surface into a hard and brittle phase. This phase easily fractures and produces debris (Fig. 12(a)). The process starts at the center of the wear track where pressure is maximized (Fig. 12(b)). Sauger [47] indicates that this phase may be called a "tribologically transformed structure". Nevertheless, for these two duplex treated samples, a total destruction of the coating was not observed as with the previous combination (Fig. 11(a)). Finally, these two samples (C2 + F101 and C2 + F102) were submitted to both oxidative and a mild abrasive wear when against alumina balls.

3.3.2.3. Duplex treated samples vs. WC ball. Fig. 13(a–b) shows the worn surfaces obtained from sliding WC balls across C1 + F101 and C1 + F102, respectively. The coatings appear to have been completely replaced with by-products of the tribological tests (Fig. 13(a)). As a matter of fact, oxide particles have agglomerated, and piled along the edges of the wear track. There are also many cracks along the wear track. The C1 + F102 duplex treated sample is not completely destroyed (Fig. 13(b)), but debris has piled at the outer edges of the wear track and there is some cracking in the middle of the track. These symptoms are indicative of adhesive and oxidative wear processes. The C2 + F101

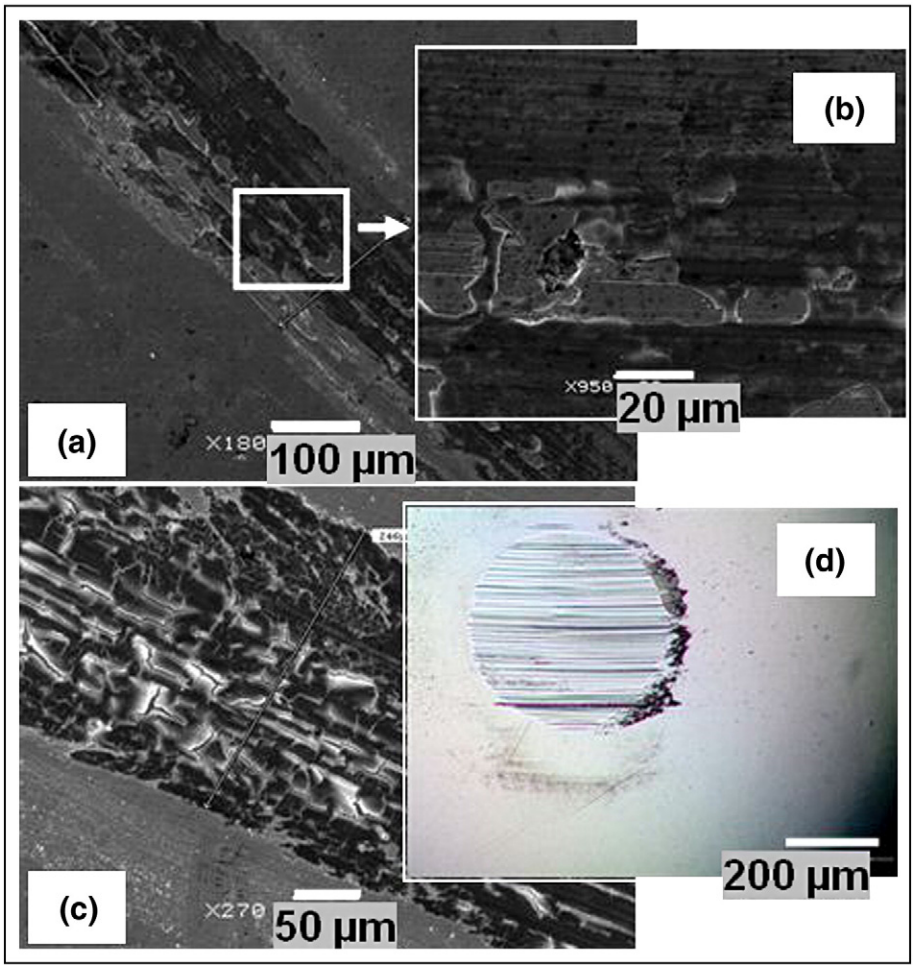

Fig. 10. Carburized samples against WC balls: C1 (a)–(b) and C2 (c) SEM images of the wear tracks, (d) optical image of the WC ball's wear scar sliding against C1 or C2.

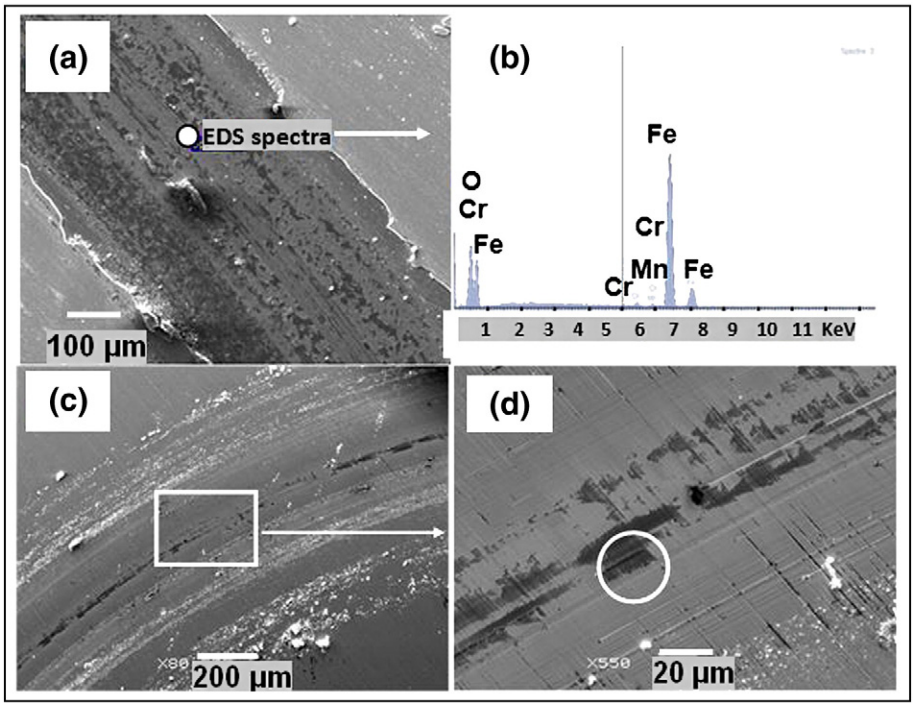

Fig. 11. Duplex treated samples against alumina ball; (a) SEM image and (b) EDS microanalysis of the wear track on C1 + F101 treated sample, (c) and (d) SEM images of the wear track on C1 + F102 treated sample.

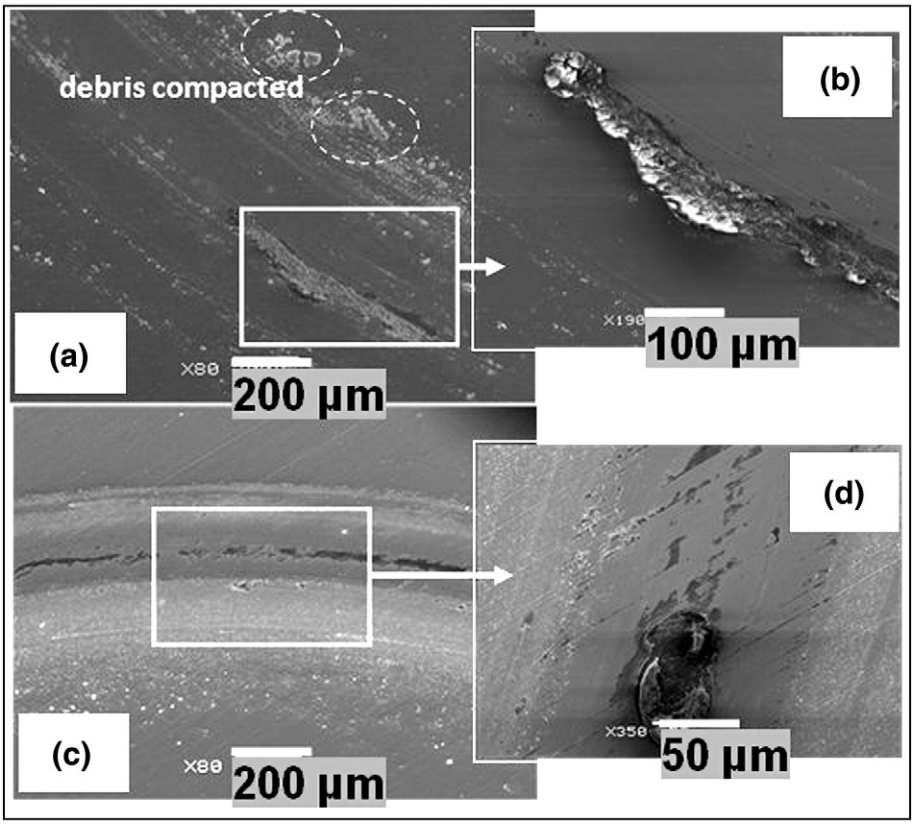

Fig. 12. SEM images of wear tracks of (a–b) C2 + F101 and (c–d) C2 + F102 duplex treated samples after sliding against alumina ball.

and C2 + F102 duplex treated samples show similar symptoms, with the presence of large debris from adhesive wear. However, it does appear that after the same sliding distance against a WC ball, the C2 + F102 (Fig. 13(d)) duplex treated sample is less worn than the C2 + F101 duplex treated sample (Fig. 13(c)).

Table 4 summarizes the different wear mechanisms observed for both the carburized and the duplex-treated samples. Oxidative and abrasive wear are the main mechanisms on most samples. However, some of the samples also show evidence for adhesive wear.

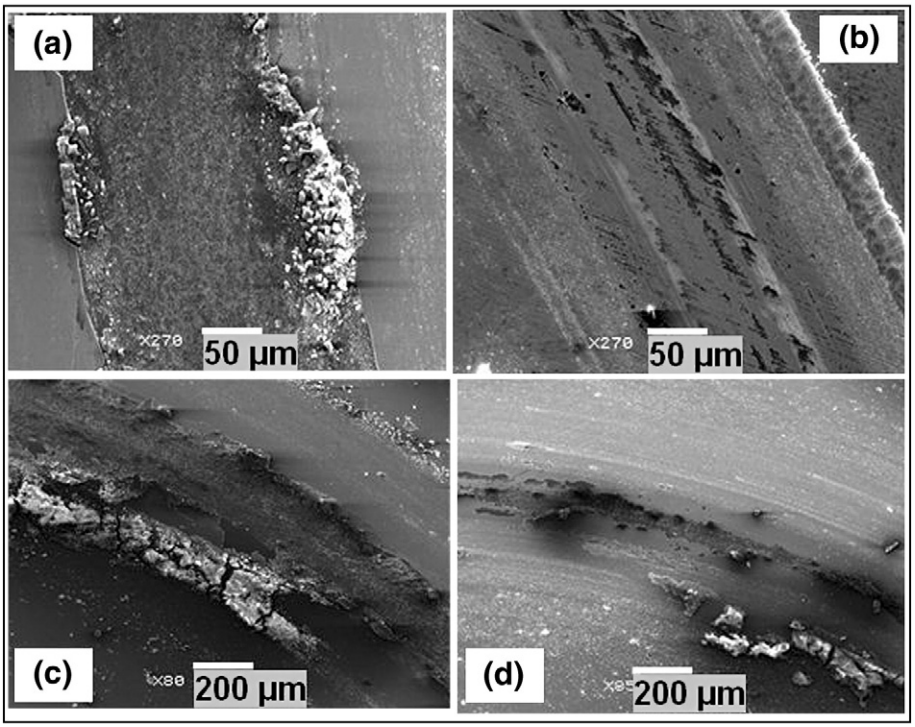

Fig. 13. SEM images of (a) C1 + F101, (b) C1 + F102, (c) C2 + F101 and (d) C2 + F102 duplex treated samples worn surface after sliding against WC ball.

Table 4
Wear mechanism of the different treatment couples.

Treatment	Counterpart	Wear mechanism	
		Disks	Balls
Carburizing	Alumina	Oxidative + abrasive	Oxidative + abrasive
C1; C2	WC	Oxidative + adhesive	Abrasive
Duplex treatments	Alumina	Oxidative + abrasive	Oxidative + abrasive
C1 + F101; C1 + F102 C2 + F101; C2 + F102	WC	Oxidative + adhesive	Abrasive

3.3.2.4. Analyses of the counterpart wear scars. Both the carburized samples (Fig. 10(d)) and the duplex treated samples (Fig. 14(a)) developed similar wear tracks on the WC balls: deep grooves, which are parallel to the sliding direction and may be due to a severe abrasive wear mechanism. The volume loss of the cemented carbide counterparts was estimated by measuring the variation of the wear track diameter (yellow circle in Fig. 14(a)) on the ball's surface.

In comparison, the wear scars of the alumina balls, which developed after sliding against carburized samples, were completely different from the ones observed after sliding against duplex treated samples. When the alumina balls were in contact with the carburized samples, their wear scars were entirely covered with a significant amount of adherent materials and scratches (stripes) (Fig. 9(d)). After sliding against the duplex treated samples, only a part of the wear scar of the alumina ball was covered by adherent material (wear product) (Fig. 14(b)). The wear scars appear relatively smooth (polished) and composed of very fine grooves. Thus, the Cr–WC coatings produced more damage on the alumina balls surface than the carburized samples (C1 or C2) and the wear mechanism seems to be abrasive. In this particular case, the volume loss was estimated by the measurement of the axes of the ellipse shown in Fig. 14(b) by optical microscopy.

3.3.3. Quantification of wear

The wear rates of the carburized and the duplex treated samples, against both alumina and cemented carbide counterparts, are shown in Fig. 15(a). The carburized samples show the highest wear rates, against either the alumina or cemented carbide counterparts, but it should be noted that the C1 process provided better wear protection than the C2 process. This may be related to the higher surface hardness of the C1 samples. The duplex treated samples showed significantly lower wear rates over the carburized samples. However, there were some differences between the two duplex treatments. When against either the alumina or cemented carbide counterparts, the surface coated with the F102 composition led to a lower wear rate than coating the surface with the F101 composition. This is supported by SEM observations of less damage on the F102 coated samples when compared to the F101 coated samples.

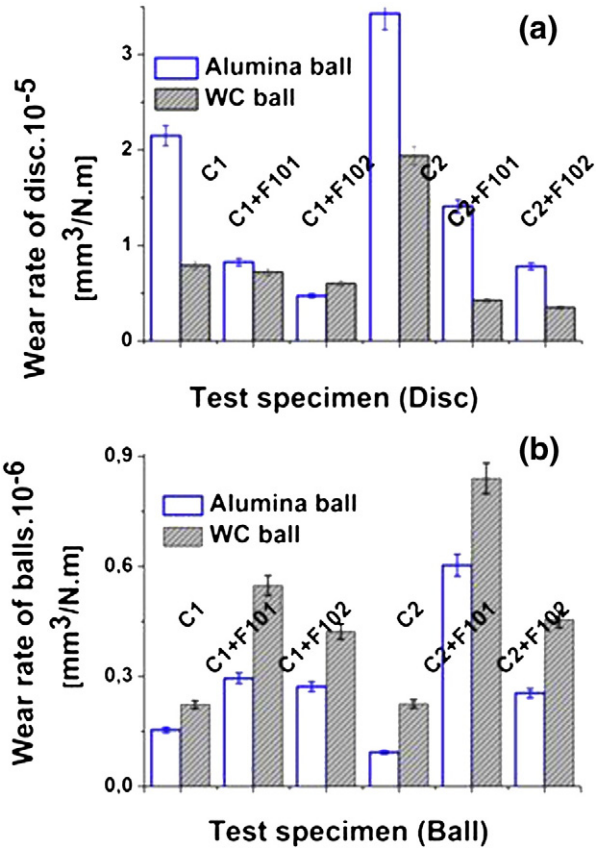

Fig. 15. Wear rates of (a) tested samples and (b) counterparts.

The counterpart wear rates are significantly smaller than the disk wear rates (Fig. 15(b).

As such, the addition of the counterpart wear to the total wear rate for each friction pair does not change the trends identified earlier in this section. Yet, despite the small ball wear rates, there are some identifiable trends. In all cases, the WC counterparts showed higher wear rates than the alumina balls.

The C2 + F101 coating versus a carbide ball caused the most significant counterpart wear. The least amount of counterpart wear occurred with an alumina ball paired against the C2 carburized sample.

From the above results and discussions, general comments can be suggested:

(i) From the point of only considering the friction behavior, the carburized process C1 and coating F102 can be considered as the best combination for either tribo-pair system (Fig. 8).
(ii) The influence of the residual stresses on the wear resistance of the coatings was not considered in this work. However, the

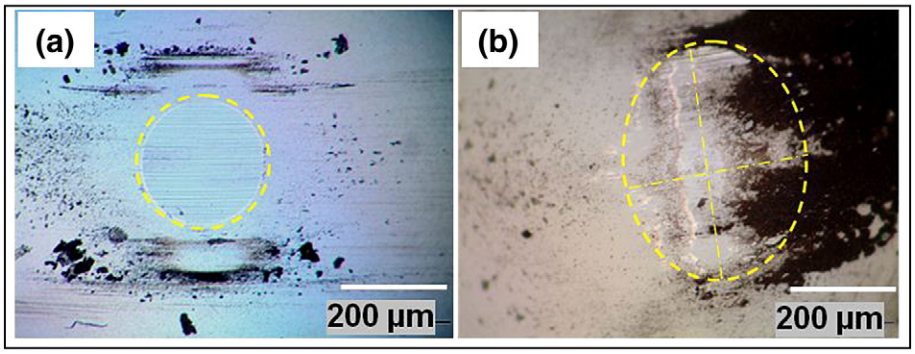

Fig. 14. Optical images of wear scars of (a) WC and (b) alumina balls after sliding against duplex treated samples.

carburizing process is well-known to induce surface stresses in steel. According to literature [48], these stresses could have a strong effect on the adherence of coatings and affect their wear resistance. Consequently, the "C2" process seems to be preferable because less carbon leads to the lowest stress level.

(iii) The F101 and F102 coatings present approximately equal mechanical properties, but the second one appears to be better crystallized. Based on SEM investigations (Figs. 11, 12 and 13), and on the wear rate results (Fig. 15), the combination (C2 + F102) seems to be the best duplex treatment under the experimental parameters used in this study.

(iv) The wear tests conducted in this study, and which represent the core of this work, showed that there were clear differences between the tribological behaviors of the coated samples when paired with alumina or cemented-WC counterparts. So in agreement with the literature [49], such differences against two different counterpart materials cannot be explained by only differences in hardness. Wear and friction is a system-response that depends on the composition, properties of the materials to be tested and also on those of the counterpart materials [12,50–52]. The wear products (debris) play a key role in the tribological behavior of the couple in contact. It was demonstrated [50] that the wear loss of the sample will be determined also by the size and shape of the hard particles presented in wear debris. So, the morphology of debris formed during the sliding of the coating against the counterpart material can reduce friction. In addition, lubricating oxides, such as Cr_2O_3, are well-known to play a main role in reducing the friction coefficient [13]: the higher the quantity of lubricating oxides, the better the wear resistance.

(v) A comparison, with other studies e.g. Cr–C system [16,18,20] has been made. It shows that the hardness and Young's modulus are in the same order. Furthermore the duplex treatments studied here, showed higher hardness regarding with the duplex treated layers of the literature such as nitriding and PVD coating [1,4] or carburizing and PVD coating [3] of low alloy steels. On the other hand, the coefficient of friction (COF) and wear rate (K) against alumina of the synthesized CrWC coatings are within the range of those of various anti-wear coatings on cutting tools for wood machining tested in the literature [36–39,42,44]. However friction coefficients of 0.5 and wear rates from $1.3 \cdot 10^{-7}$ $mm^3/N \cdot m$ to $7 \cdot .10^{-7}$ $mm^3/N \cdot m$ against alumina balls are reported by A. Gilewicz et al. [36] for high-speed steel tools applied for wood processing. Recently, wear behavior and cutting performance of nanostructured hard coatings were investigated [41]; the obtained wear rate against alumina balls was in the range of 7×10^{-6} $mm^3/N \cdot m$–9×10^{-6} $mm^3/N \cdot m$. So, this study clearly suggests the possibility of extending the use of duplex treatments also on low-alloy steels instead of the commonly used tool steels.

4. Conclusion

The objective of our current work is the development of optimized surface treatment processes for wood cutting tools. With this paper, the wear behavior of a duplex surface treatment of low carbon steel was elucidated. The process involves low pressure carburizing and the deposition of a Cr–(WC–Co) coating via RF magnetron sputtering. The tribological and wear behaviors of the carburized and duplex treated samples can be summarized as follows:

- During the run-in phase of the tribological tests, the carburized samples showed the lowest coefficients of friction against both alumina and cemented carbide counterparts. However, by the end of the 2000 cycle test, the duplex-treated samples showed slightly lower friction coefficients.
- Duplex treated samples have lower wear rates than the carburized samples of low alloy steel. The F102 coating, with its lower Cr:W ratio, showed better wear resistance than the F101 coated samples.
- The primary wear mechanism for all samples was oxidative. The amount of wear debris at the interface between the friction pairs seems to play a role in determining the presence of other wear mechanisms, such as adhesive and/or abrasive.

The next step will be the study of the tribological and wear behaviors of these carburized and duplex treated samples against wood counterparts. Specifically, beech is of great interest. This is a very common species of wood in Europe, and it is used in a wide variety of applications.

Acknowledgments

The authors would like to thank Dr. A. ZAIRI for the nanoindentation and scratch tests; Mr. D. LAGADRILLÈRE for the SEM-EDS observations (Arts et Métiers ParisTech of Cluny and Lille-France), and Dr. Yujiao ZOU and Dr. Andrei V. STANISHEVSKY for the XRD analyses (University of Alabama at Birmingham, USA).

References

[1] G.M. LaVecchia, N. Lecis, Surf. Coat. Technol. 205 (2010) 614–619.
[2] I. Zukerman, A. Raveh, Y. Landau, R. Weiss, R. Shneck, Y. Shneor, Surf. Coat. Technol. 201 (2007) 6171–6175.
[3] B.S. Saini, V.K. Gupta, Surf. Coat. Technol. 205 (2010) 511–518.
[4] C.A. Llanes Leyva, C. Godoy, A.C. Bozzi, J.C. Avelar-Batista Wilson, Surf. Coat. Technol. 206 (2011) 1796–1808.
[5] A. Topuz, D. Toplu, Prakt. Metallogr. 36 (1999) 5–12.
[6] S. Taktak, S. Ulker, I. Gunes, Surf. Coat. Technol. 202 (2008) 3367–3377.
[7] F. Hakami, M. Heydarzadeh Sohi, J. Rasizadeh Ghani, Thin Solid Films 519 (2011) 6792–6796.
[8] O. Kessler, Surf. Coat. Technol. 201 (2006) 4046–4051.
[9] O. Kessler, F.T. Hoffmann, P. Mayr, Surf. Coat. Technol. 108–109 (1998) 211–216.
[10] C. Nouveau, C. Labidi, J.P. Ferreira Martin, R. Collet, A. Djouadi, Wear 263 (2007) 1291–1299.
[11] Y. Zou, M.J. Walock, S.A. Catledge, C. Nouveau, A. Stanishevsky, J. Achiev. Mater. Manuf. Eng. 37 (2009) 369–374.
[12] Lorenzo-Martin, O. Ajayi, A. Erdemir, G.R. Fenske, R. Wie, Wear 302 (2013) 963–1071.
[13] L. Wang, X. Nie, J. Mater. Eng. Perform. 23 (2014) 560–571.
[14] T. Polcar, T. Vitu, L. Cvrcek, J. Vyskocil, A. Cavaleiro, Tribol. Int. 43 (2010) 1228–1233.
[15] Y.-S. Yang, W. Huang, W.Y. Huang, Thin Solid Films 519 (2011) 4899–4905.
[16] M. Andersson, J. Högström, S. Urbonaite, A. Furlan, L. Nyholm, U. Jansson, Vacuum 86 (2012) 408–1416.
[17] Y.L. Su, T.H. Liu, C.T. Su, T.P. Cho, Mater. Sci. Eng. A 364 (2004) 188–197.
[18] A. Jellad, S. Labdi, T. Benameur, J. Alloys Compd. 483 (2009) 464–467.
[19] A. Paul, J. Lim, K. Choi, C. Lee, Mater. Sci. Eng. A 332 (2002) 123–128.
[20] M.A. Gomez, J. Romero, A. Lousa, J. Esteve, Surf. Coat. Technol. 200 (2005) 1819–1824.
[21] C. Ziebert, J. Yea, M. Stüber, S. Ulrich, M. Edinger, I. Barzen, Surf. Coat. Technol. 205 (2011) 4844–4849.
[22] Y. Wu, S. Hong, J. Zhang, Z. He, W. Guo, Q. Wang, et al., Int. J. Refract. Met. Hard Mater. 32 (2012) 21–26.
[23] P. Jacquet, D.R. Rousse, G. Bernard, M. Lambertin, Mater. Chem. Phys. 77 (2002) 542–551.
[24] ASTM G 99 –95c, Standard test method for wear testing with a Pin-on-Disk apparatus, 1995.
[25] R. Ramadoss, N. Kumar, S. Dash, D. Arivuoli, A.K. TyagiInt, Int. J. Refract. Met. Hard Mater. 41 (2013) 547–552.
[26] L. Wang, J. Zhou, J. Duszczyk, L. Katgerman, Tribol. Int. 50 (2012) 66–75.
[27] N.E. Beliardouh, K. Bouzid, C. Nouveau, B. Tlili, M.J. Walock, Tribol. Int. (2014), http://dx.doi.org/10.1016/j.triboint.2014.03.018i.
[28] J.F. Archard, W. Hirst, Proc. R. Soc. Lond. A 236 (1956) 397–410.
[29] J.F. Archard, J. Appl. Phys. 24 (8) (1953) 981–988.
[30] J. Qu, J.J. Truhan, Wear 261 (2006) 848–855.
[31] C.A. Stickels, ASM Handbooks, Volume 18, Surface Treatments and Coatings for Friction and Wear Control, 1992.
[32] M.J. Walock, I. Rahil, Y. Zou, L. Imhoff, S.A. Catledge, C. Nouveau, et al., J. Nanosci. Nanotechnol. 12 (2012) 4825–4831.
[33] Standard Terminology Relating to Wear and Erosion, Annual Book of ASTM Standards, G 40, 1989.
[34] J. Rech, C. Claudin, E. D'Eramo, Tribol. Int. 42 (2009) 738–744.
[35] K. Chu, P.W. Shum, Y.G. Shen, Mater. Sci. Eng. B 131 (2006) 62–71.
[36] A. Gilewicz, B. Warcholinskia, P. Myslinskia, W. Szymanskib, Wear 270 (2010) 32–38.
[37] M.G. Faga, L. Settineri, Surf. Coat. Technol. 201 (2006) 3002–3007.
[38] D. Zhang, B. Shen, F. Sun, Appl. Surf. Sci. 256 (2010) 2479–2489.

[39] L. Settineri, M.G. Faga, G. Gautier, M. Perucca, CIRP Ann. Manuf. Technol. 57 (2008) 575–578.
[40] L. Wang, X. Lei, B. Shen, F. Sun, Z. Zhang, Diam. Relat. Mater. 33 (2013) 54–62.
[41] H. Calıskan, C. Kurbanoglu, P. Panjan, M. Cekada, D. Kramar, Tribol. Int. 62 (2013) 215–222.
[42] F. Eblagon, B. Ehrle, T. Graule, J. Kuebler, J. Eur. Ceram. Soc. 27 (2007) 419–428.
[43] A. Gilewicz, B. Warcholinski, W. Szymanski, W. Grimm, Tribol. Int. 57 (2013) 1–7.
[44] L. Settineri, M.G. Faga, Wear 260 (2006) 326–332.
[45] J.L. Mo, M.H. Zhu, Tribol. Int. 41 (2008) 1161–1168.
[46] J.L. Mo, M.H. Zhu, Wear 267 (2009) 874–881.
[47] E. Sauger, Contribution à l'étude de la transformation tribologique superficielle en fretting(PhD Thesis) Ecole Centrale de Lyon, France, 1997. (N° 97-25).
[48] E.E. Vera, M. Vite, R. Lewis, E.A. Gallardo, J.R. Laguna-Camacho, Wear 271 (2011) 2116–2124.
[49] Y.J. Kim, T.J. Byun, J.G. Han, Superlattice. Microst. 45 (2009) 73–79.
[50] C.X. Li, J. Xia, H. Dong, Wear 261 (2006) 693–701.
[51] Y.H. Cheng, T. Browne, B. Heckerman, Wear 271 (2011) 775–782.
[52] G.A. Fontalvo, R. Daniel, C. Mitterer, Tribol. Int. 43 (2010) 108–112.